混合配体构筑的两个锌(II)和镉(II)的金属有机框架化合物的合成、晶体结构及吸附和荧光性质

李玉玲 [1,2]　赵　越 [*,1]　孙为银 [1]

([1] 南京大学化学化工学院，配位化学国家重点实验室，南京　210023)
([2] 郑州工程技术学院化工食品学院，郑州　450044)

摘要： 在溶剂热条件下，由 1,3,5-三(1-咪唑基)苯(tib)和 3,4′,5-联苯三羧酸(H₃BPT)或 1,3,5-三(4-羧基苯基)苯(H₃BTB)与镉的硝酸盐或锌的硝酸盐反应，得到 2 个新的金属有机框架化合物[Cd₃(tib)₂(BPT)₂(H₂O)₂]·DMA·6H₂O (**1**)和[Zn₂(tib)(HBTB)₂(H₂O)]·2H₂O (**2**)，并对其结构和吸附及荧光性能进行了研究。结构分析结果表明配合物 **1** 是一个具有 4 节点的三维框架化合物，其简化后的拓扑符号为{8³}₄{8⁵·12}{8⁶}₂；而 **2** 是一个具有二维网格结构的化合物，该二维网格结构可进一步通过氢键作用形成三维超分子化合物。气体和蒸汽吸附性能研究结果表明 **1** 和 **2** 都可以选择性吸附 CO₂ 和 MeOH，荧光性能研究结果表明，**1** 可以通过荧光猝灭机理在甲醇、乙醇、2-异丙醇、乙腈、*N,N*-二甲基甲酰胺、*N,N*-二甲基乙酰胺、四氢呋喃、三氯甲烷、二氯甲烷和丙酮的混合溶剂中选择性识别丙酮分子。

关键词： 锌(II)/镉(II)的金属有机框架化合物；吸附性能；荧光性能

Two Zn(II) and Cd(II) Metal-Organic Frameworks with Mixed Ligands: Synthesis, Structure, Sorption and Luminescent Properties

LI Yu-Ling[1,2]　ZHAO Yue[*,1]　SUN Wei-Yin[1]

([1] *State Key Laboratory of Coordination Chemistry, School of Chemistry and Chemical Engineering, Nanjing University, Nanjing 210023, China*)
([2] *School of Chemical Engineering and Food Science, Zhengzhou University of Technology, Zhengzhou 450044, China*)

Abstract: Two new metal-organic frameworks (MOFs) [Cd₃(tib)₂(BPT)₂(H₂O)₂]·DMA·6H₂O (**1**) and [Zn₂(tib)(HBTB)₂(H₂O)]·2H₂O (**2**) (tib=1,3,5-tris(1-imidazolyl)benzene, H₃BPT=biphenyl-3,4′,5-tricarboxylic acid, H₃BTB=4,4′,4″-benzene-1,3,5-triyl-tribenzoic acid, DMA=*N,N*-dimethylacetamide) were synthesized and characterized. Complex **1** is a 4-nodal three-dimensional (3D) framework with point symbol {8³}₄{8⁵·12}{8⁶}₂, while **2** is a two-dimensional (2D) network to be joined together by hydrogen bonds to generate a 3D supramolecular structure. Gas/vapor adsorption and luminescence behavior of the two complexes were studied. It is meaningful that **1** and **2** can selectively adsorb CO₂ over N₂, and MeOH over EtOH. Furthermore, **1** can selectively detect acetone through a fluorescence quenching mechanism in the organic solvents including MeOH, EtOH, 2-PA, CH₃CN, DMF, DMA, THF, CHCl₃, CH₂Cl₂ and acetone. CCDC: 1996242, **1**; 1845264, **2**.

Keywords: Zn(II) and Cd(II) MOFs; sorption properties; luminescent properties

Over the past years, the rational design and synthesis of functional metal-organic frameworks (MOFs) materials have caused remarkable attention due to their rich and varied structures as well as potential application, such as gas storage and separation, magnetism, heterogeneous catalysis, drug delivery and luminescence[1-8]. However, it still remains challenging by control-synthesizing and predicting structures of the functional MOFs because of many factors which can affect the structures and properties of MOFs. Among these factors, the selection of organic linkers is very crucial for formation of MOFs with definite framework structures and desired properties. Therefore, proper organic bridging linkers are significant in building the desired MOFs materials. As for as we know, biphenyl-3,4′,5-tricarboxylic acid (H$_3$BPT) and 4,4′,4″-benzene-1,3,5-triyl-tribenzoic acid (H$_3$BTB) (Scheme 1) are good bridging ligands because of their diversified coordination modes and rigid multicarboxylic groups[9-12].
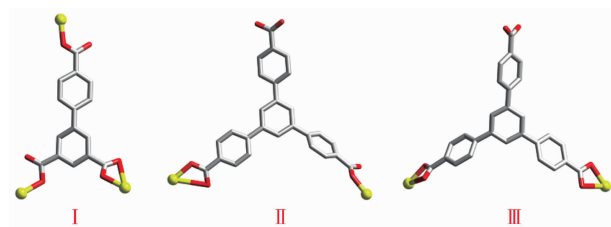
Scheme 1　Coordination modes of BPT^{3-} and HBTB^{2-} in **1** and **2**

In our previous studies, a rigid tridentate ligand 1,3,5-tris(1-imidazolyl)benzene (tib) as a N-donor ligand have been used in construction of MOFs, and the results showed that it can react with varied metal salts leading to the formation of MOFs with specific structures and interesting properties[13-15]. Thus, it is meaningful for using mixed N-donor ligand tib and multicarboxylic acids H$_3$BPT/H$_3$BTB to construct MOFs with novel structures and properties. In this work, two new metal-organic frameworks, [Cd$_3$(tib)$_2$(BPT)$_2$(H$_2$O)$_2$]·DMA·6H$_2$O (**1**) and [Zn$_2$(tib)(HBTB)$_2$(H$_2$O)]·2H$_2$O (**2**) (tib=1,3,5-tris(1-imidazolyl)benzene, H$_3$BPT=biphenyl-3,4′,5-tricarboxylic acid, H$_3$BTB=4,4′,4″-benzene-1,3,5-triyl-tribenzoic acid, DMA=*N,N*-dimethylacetamide), were synthesized and character-

ized. Structural characterization reveals that complex **1** is a 4-nodal 3D framework with point symbol {8^3}$_4$ {8^5·12}{8^6}$_2$, while **2** is a 2D network to be joined together by hydrogen bonds to generate a 3D supramolecular structure. Gas/vapor adsorption and luminescence behavior of the two complexes were studied. It is meaningful that **1** and **2** can selectively adsorb CO$_2$ over N$_2$, and MeOH over EtOH. Furthermore, **1** can selectivity detect acetone through a fluorescence quenching mechanism in the organic solvents including MeOH, EtOH, 2-PA, CH$_3$CN, DMF, DMA, THF, CHCl$_3$, CH$_2$Cl$_2$ and acetone.

1　Experimental

1.1　Materials and measurements

All commercially available chemicals and solvents are of reagent grade and were used as received without further purification. Ligand tib was prepared according to the procedures reported previously [16]. Elemental analyses for C, H and N were performed on a FLASH EA 1112 elemental analyzer. Thermogravimetric analyses (TGA) were carried out on a Mettler-Toledo (TGA/DSC1) thermal analyzer under nitrogen with a heating rate of 10 ℃·min^{-1}. FT-IR spectra were recorded in a range of 400~4 000 cm^{-1} on a BRUKER TENSOR 27 spectrophotometer using KBr pellets. Powder X-ray diffraction (PXRD) analyses were performed on a Bruker D8 Advance X-ray diffracto-meter with Cu $K\alpha$ (λ=0.154 18 nm) radiation, in which the X-ray tube was operated at 40 kV and 40 mA, and the scanning angle range was between 5° and 50°. Sorption experiments were carried out on a Belsorp-max volumetric gas sorption instrument. The lumine-scence spectra were recorded on an Aminco Bowman Series 2 spectrofluorometer with a xenon arc lamp as the light source. The pass width of 10 nm was used in the measurements of emission and excitation spectra, and all the measurements were performed under the same experimental conditions.

1.2　Synthesis of [Cd$_3$(tib)$_2$(BPT)$_2$(H$_2$O)$_2$]·DMA· 4H$_2$O (1)

A mixture of tib (13.8 mg, 0.05 mmol), H$_3$BPT (14.3 mg, 0.05 mmol), and Cd(NO$_3$)$_2$·4H$_2$O (30.0 mg,

0.1 mmol) in DMA/H$_2$O (8 mL, 3∶1, V/V) was placed in an 18 mL Teflon-lined stainless steel container and heated at 90 ℃ for 72 h. Thereafter, colorless block-shaped crystals of **1** were isolated in 80% yield (based on tib). Elemental analysis Calcd. for C$_{64}$H$_{63}$N$_{13}$O$_{21}$Cd$_3$ (%): C 45.55, H 3.76, N 10.79; Found(%): C 45.28, H 3.91, N 10.72. IR (KBr pellet, cm^{-1}): 3 357 (m), 3 143 (m), 1 670 (m), 1 610 (m), 1 569 (s), 1 403 (s), 1 357 (m), 1 278 (m), 1 191 (m), 1 096 (m), 1 051 (m), 932 (m), 852 (m), 792 (s), 674 (m), 558 (m), 447 (m).

1.3 Synthesis of [Zn$_2$(tib)(HBTB)$_2$(H$_2$O)]·2H$_2$O (2)

Complex **2** was synthesized by tib (13.8 mg, 0.05 mmol), H$_3$BTB (22.0 mg, 0.05 mmol) and Zn(NO$_3$)$_2$· 6H$_2$O (30.0 mg, 0.1 mmol) in H$_2$O (8 mL) in a 18 mL glass vial and heated at 160 ℃ for 72 h. After cooling to room temperature, colorless block crystals of **2** were obtained with a yield of 75% based on tib. Anal. Calcd. for C$_{69}$H$_{50}$N$_6$O$_{15}$Zn$_2$ (%): C 62.13, H 3.78, N 6.30; Found(%): C 62.07, H 3.85, N 6.25. IR (KBr pellet, cm^{-1}): 3 449 (m), 1 689 (s), 1 662 (s), 1 620 (s), 1 511 (m), 1 401 (s), 1 240 (m), 1 177 (m), 1 075 (s), 1 015 (s), 946 (m), 854 (m), 774 (s), 683 (m), 646 (m), 482 (m).

1.4 Sample activation

Solvent-exchanged samples were prepared by immersing the as-synthesized samples **1** in THF for 3 days to remove the nonvolatile solvates, the solvent was decanted every 8 h, and fresh THF was added. The activated sample **1′** was obtained by heating the solvent-exchanged samples at 423 K under a dynamic high vacuum for 10 h. The activated samples **2′** was obtained by heating the sample **2** directly at 423 K under a dynamic high vacuum for 10 h.

1.5 X-ray crystallography

Crystallographic data of **1** and **2** were collected on a Bruker Smart Apex Ⅱ CCD area-detector diffra-

ctometer with graphite-monochromated Mo Kα radiation (λ =0.071 073 nm) using the ω-scan technique. The diffraction data were integrated using the SAINT program[17], which were also used for the intensity corrections for the Lorentz and polarization effects. Semi-empirical absorption correction was applied using the SADABS program[18]. Complex **1** was solved by direct methods using SHELXT-2014 and all the non-hydrogen atoms were refined anisotropically on F^2 by the full-matrix least-squares technique with the SHELXL-2018[19-20]. Complex **2** was solved by direct methods using SHELXT-2014 and all the non-hydrogen atoms were refined anisotropically on F^2 by the full-matrix least-squares technique with the SHELXL-2014[19]. All the hydrogen atoms, except for those of water molecules, were generated geometrically and refined isotropically using the riding model. The hydrogen atoms of the coordinated water molecules were found from the Fourier map directly, while those of free water molecules were not found. Because some free solvent molecules in **1** are highly disordered and impossible to refine using conventional discrete-atom models, the SQUEEZE subroutine of the PLATON software suite[21-22] was applied to remove the scattering from the highly disordered solvent molecules. The formula of **1** was calculated based on volume/count _electron analysis, thermogravimetric analysis (TGA) and elemental analysis. The reported refinements are of the guest-free structures obtained by the SQUEEZE routine, and the results are attached to the CIF file. The details of the crystal parameters, data collection, and refinements for the **1** and **2** are listed in Table 1. Selected bond lengths and angles are given in Table S1, and the hydrogen bond data for **2** are provided in Table S2.

CCDC: 1996242, **1**; 1845264, **2**.

Table 1 Crystal data and structure refinements for 1 and 2

Complex	1	2
Formula	C$_{64}$H$_{63}$N$_{13}$O$_{21}$Cd$_3$	C$_{69}$H$_{50}$N$_6$O$_{15}$Zn$_2$
Formula weight	1 687.47	1 333.89
T / K	296(2)	293(2)
Crystal system	Monoclinic	Triclinic

Continued Table 1

	$C2/c$	$P\bar{1}$
Space group	$C2/c$	$P\bar{1}$
a / nm	2.470 8(6)	1.093 6(5)
b / nm	1.382 6(3)	1.678 9(5)
c / nm	2.443 7(5)	1.946 5(5)
α / (°)		115.401(5)
β / (°)	113.117(4)	90.811(5)
γ / (°)		103.052(5)
V / nm³	7.678(3)	3.119 8(19)
Z	4	2
D_c / (g·cm⁻³)	1.460	1.420
$F(000)$	3 400	1 372
θ for data collection / (°)	1.724~27.367	1.361~24.998
Reflection collected	24 621	10 832
Unique reflection	8 603	8 061
Goodness-of-fit on F^2	1.011	0.902
$R_1{}^a$ [$I>2\sigma(I)$]	0.046 0	0.053 5
$wR_2{}^b$ [$I>2\sigma(I)$]	0.101 2	0.160 0

^{a} $R_1 = \sum \|F_o\|-\|F_c\|\| / \sum \|F_o\|$; ^{b} $wR_2 = |\sum w(|F_o|^2-|F_c|^2)| / \sum |w(F_o)^2|^{1/2}$, where $w=1/[\sigma^2(F_o^2)+(aP)^2+bP]$, $P=(F_o^2+2F_c^2)/3$.

2　Results and discussion

2.1　Crystal structure of [Cd₃(tib)₂(BPT)₂(H₂O)₂]· DMA·6H₂O (1)

X-ray crystallographic analyses show that **1** crystallizes in the $C2/c$ space group (Table 1). As shown in Fig.1a, the asymmetric unit of **1** contains two crystallographically independent Cd(Ⅱ) cations, which have different coordination environments. The Cd1 is in a distorted tetrahedral coordination geometry with two N atoms (N1, N1A) from two different tib ligands and two carboxylate O atoms (O1, O1A) from two distinct BPT³⁻ anions, while the Cd2 is six-coordinated with a distorted octahedral geometry by two imidazole N atoms (N6B, N4C) from two different tib ligands, three carboxylate O atoms (O3D, O4D, O5) from two different BPT³⁻ anions, and one coordinated water molecule. The Cd-N and Cd-O bond lengths are found to be 0.227 7(3)~0.236 0(3) and 0.217 7(3)~0.248 0(3) nm, respectively (Table S1). Moreover, the coordination angles around Cd are in a range of 55.12(8)°~178.81(12)° (Table S1). In **1**, each Cd(Ⅱ) ion connects two tib and every tib joins three Cd(Ⅱ) ions to form a 2D network (Fig.1b). Meanwhile, each BPT³⁻ ligand

adopts the coordination mode (κ^1)-(κ^1)-(κ^2)-μ_3-BPT coordination mode (Scheme 1, mode Ⅰ) to connect three Cd(Ⅱ) cations and every Cd(Ⅱ) links two ligands to build a 2D Cd-BPT structure (Fig.1c). The 2D Cd-tib and 2D Cd-BPT are interspersed with Cd ions as nodes to generate the final 3D structure (Fig.1d). According to the simplification principle, Cd1, Cd2, tib, and BPT³⁻ can be viewed as four-, four-, three-, and three-connectors, respectively. So, the resulting structure of **1** is a (3, 3, 4, 4)-connected 4-nodal 3D framework with a $\{8^3\}_4\{8^5·12\}\{8^6\}_2$ topology (Fig.1e)[23]. Additionally, the solvent-accessible volume of **1** is 2.025 4 nm³ per 7.338 4 nm³ unit cell volume (27.6% of the total crystal volume)[24].

2.2　Crystal structure of [Zn₂(tib)(HBTB)₂(H₂O)]· 2H₂O (2)

When the H₃BPT was replaced by H₃BTB, complex **2** was isolated. As illustrated in Fig.2a, the asymmetric unit of **2** contains two crystallographically independent Zn ions. Zn1 is six-coordinated with distorted octahedral geometry by two imidazole N atoms (N1, N5A) from two different tib and four carboxylate O ones (O1, O2, O7, O8) from two distinct HBTB²⁻, with Zn1-N bond distance from 0.201 9(3) to
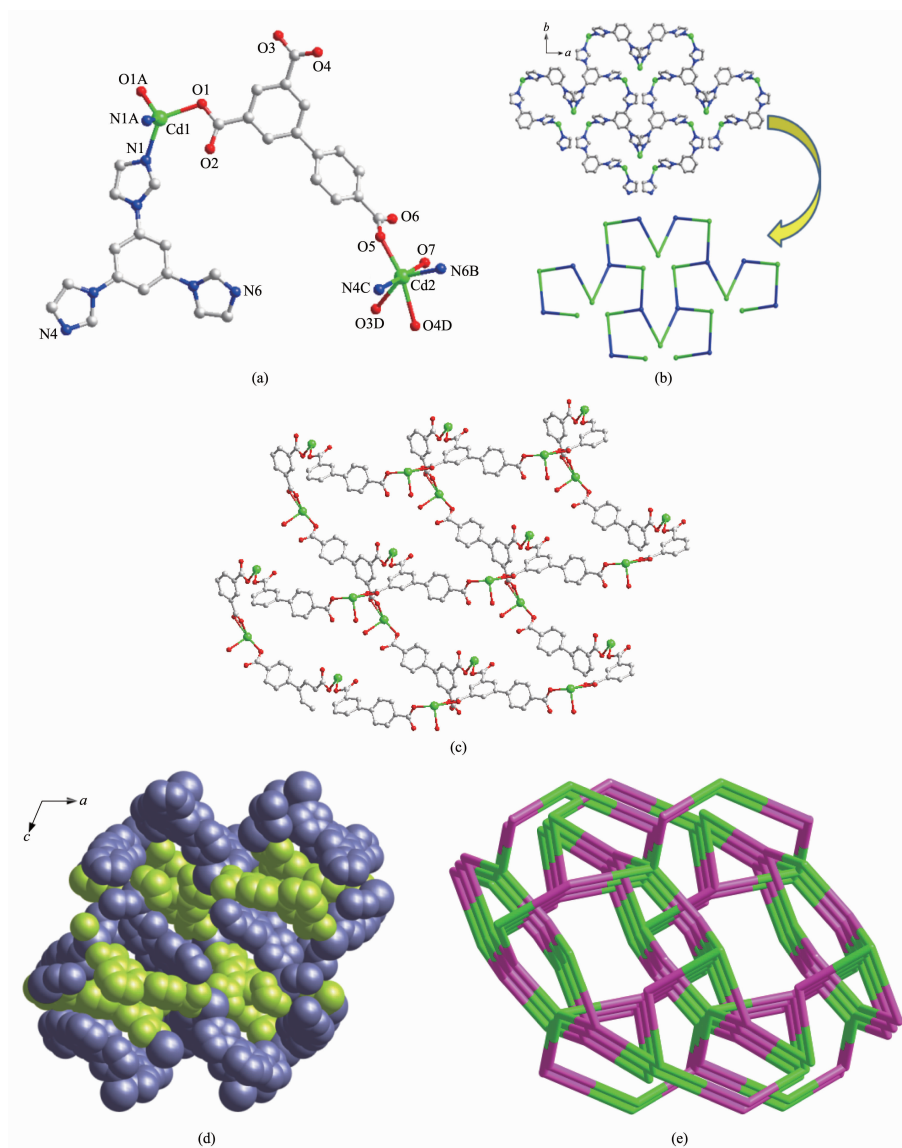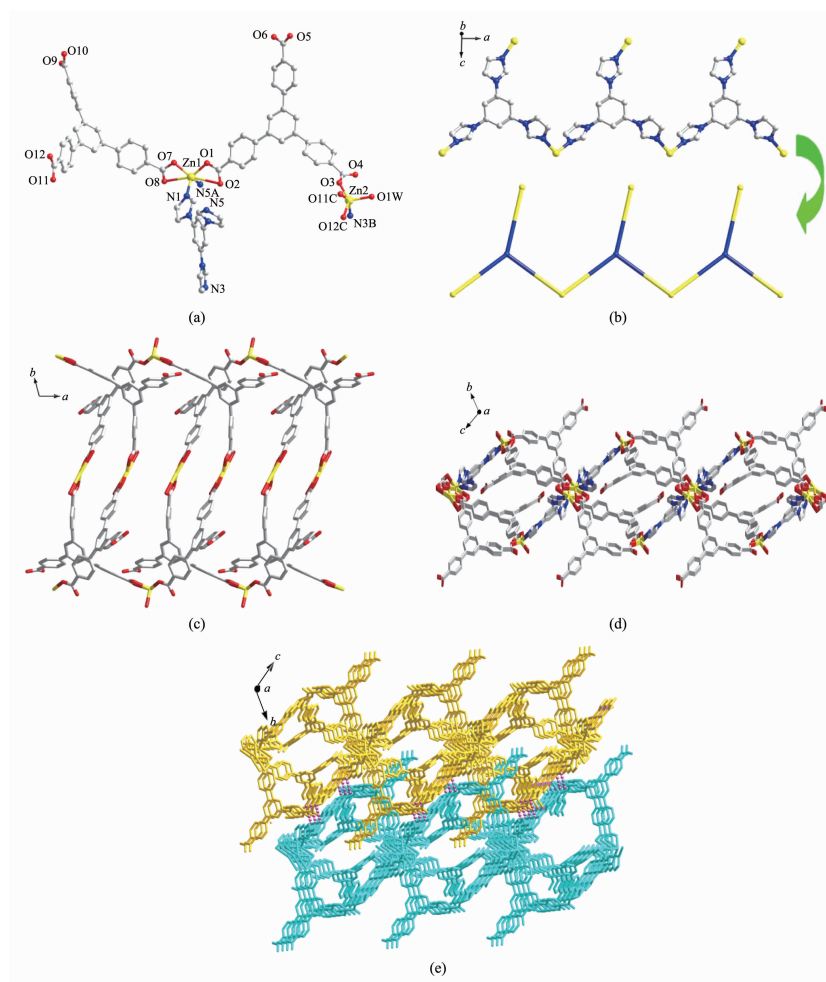
Hydrogen atoms and free solvent molecules are omitted for clarity; Symmetry codes: A: −x+2, y, −z+3/2;
B: −x+1, −y+1, −z+1; C: x−1/2, −y+3/2, z−1/2; D: x−1/2, y+1/2, z

Fig.1 (a) Coordination environment around Cd(Ⅱ) in **1**; (b) 2D Cd-tib network in **1**; (c) 2D Cd-BPT network
structure in **1**; (d) 3D packing structure of **1** (Grey color: 2D Cd-tib network, Green color: 1D Cd-BPT
chain structure); (e) Topological presentation of **1**

0.202 3(4) nm and the Zn1-O one from 0.196 2(3) to
0.198 2(3) nm. Furthermore, the coordination angles
around Zn1 are in the scope of 97.54(13)°~121.79(15)°
(Table S1). While Zn2 is five-coordinated by one
imidazole N atom (N3B) from tib ligand, three
carboxylate O atoms (O3, O11C, O12C) from different
HBTB²⁻ and one terminal water molecule (O1W). The
bond lengths and coordination angles around Zn2 are
in normal range (Table S1). In **2**, each Zn1 ions joins
two tib molecules and each tib ligand connects two

Zn1 ions to construct a 1D chain (Fig.2b). Meanwhile,
partly deprotonated HBTB²⁻ ligand adopts (κ^1)-(κ^2)-μ_2-
HBTB or (κ^2)-(κ^2)-μ_2-HBTB coordination mode (Scheme
1, mode Ⅱ and Ⅲ) to connect two Zn(Ⅱ) ions to form
a 1D chain structure (Fig.2c). The combination of 1D
Zn-tib chain and 1D Zn-HBTB chain generate a final
2D network structure of **2** (Fig.2d). Eventually,
hydrogen bonding C(10)−H(10A)···O1W and C(3)−
H(3)···O11 (Table S2) bridge the layers to form a 3D
supramolecular structure of **2** (Fig.2e).

Hydrogen atoms and free solvent molecules are omitted for clarity; Symmetry codes: A: *x*+1, *y*, *z*; B: *x*, *y*+1, *z*+1; C: −*x*, −*y*+1, −*z*

Fig.2　(a) Coordination environment of Zn(Ⅱ) in **2**; (b) 1D chain structure of Zn-tib in **2** along *b* axis; (c) 1D chain structure of Zn-HBTB in **2** along *c* axis; (d) 2D layer structure of **2**; (e) 3D supramolecular structure of **2** with hydrogen bonds indicated by dashed lines

2.3　Powder X-ray diffraction (PXRD) and thermal stability

The purity for the bulky samples of synthesized **1** and **2** were confirmed by PXRD tests and the results are provided in Fig.S1. Each PXRD pattern of the as-prepared sample was well consistent with the simulated one, confirming the phase purity of the products.

Thermogravimetric analysis (TGA) was carried out in evaluating the thermal stability of the frameworks and the TGA curves of **1** and **2** are shown in Fig.S2. Complex **1** showed a weight loss of 13.2% between 30 and 245 ℃ corresponding to the removal of free and coordinated H_2O molecules as well as free DMA molecules (Calcd. 13.4%). Further weight loss was observed at about 350 ℃, implying collapse of

the framework of complex **1** (Fig.S2a). TGA curve of **2** gave weight loss of 4.4% from 30 to 185 ℃, originating from the loss of two free and one coordinated H_2O molecules (Calcd. 4.0 %), and the framework is stable up to about 395 ℃ (Fig.S2b).

2.4　Gas and vapor adsorption properties

The porosity and high stability of the frameworks prompted us to examine their gas/vapor sorption behavior. The sorption performances of the activated samples **1′** and **2′** for N_2 at 77 K, CO_2 at 195 K, MeOH and EtOH at 298 K are discussed here.

From the Fig.3a, we can see the adsorption isotherm of N_2 at 77 K for **1′**, which suggests only surface adsorption[25]. However, as shown in Fig.3a and 3b, the adsorption capacities of CO_2, MeOH, and

EtOH on **1′** are considerable. The CO_2 adsorption capacity of **1′** at 195 K and 100 kPa was 81.12 $cm^3 \cdot g^{-1}$, corresponding to about 5.8 CO_2 molecules per formula unit, while the uptake amount of CH_3OH and CH_3CH_2OH at 298 K and 100 kPa was 105.81 $cm^3 \cdot g^{-1}$ (151.04 $mg \cdot g^{-1}$) and 33.32 $cm^3 \cdot g^{-1}$ (68.54 $mg \cdot g^{-1}$), corresponding to 7.6 MeOH molecules and 2.4 EtOH molecules per formula unit, respectively. The observed hysteretic adsorption and incomplete desorption behavior suggest strong interactions between adsorbed CO_2 and the framework[26-29]. Considering all of the above analysis results, it can be seen that complex **1** can selectively adsorb CO_2 and MeOH molecules.

It is noteworthy that almost no adsorption of N_2 at 77 K and EtOH at 298 K was found for **2′** (Fig.4a and 4b). The final value of CO_2 adsorption at 195 K and 100 kPa was 32.14 $cm^3 \cdot g^{-1}$ corresponding to about 1.9 CO_2 molecules per formula unit for **2′**. As for MeOH adsorption of **2′** at 298 K (Fig.4b), the final value of 47.3 $cm^3 \cdot g^{-1}$ (71.8 $mg \cdot g^{-1}$) at 100 kPa corresponds to 2.8 MeOH molecules per formula unit for **2′**. The hysteresis and incomplete desorption suggest the strong interactions between the adsorbate and adsorbent, which include the hydrogen bond interactions between the guest molecules and framework, as well as the guest molecules and the guest molecules.
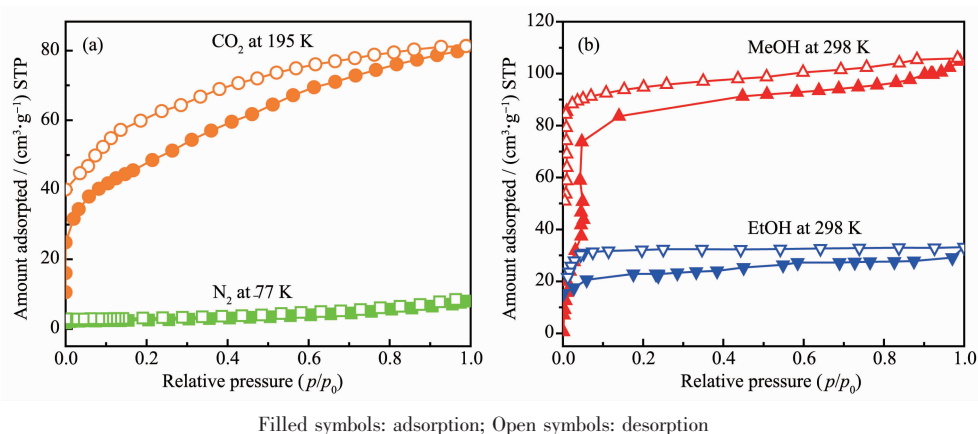

Filled symbols: adsorption; Open symbols: desorption

Fig.3　(a) Sorption isotherms of N_2 at 77 K and CO_2 at 195 K for **1′**; (b) Sorption isotherms of MeOH and EtOH at 298 K for **1′**

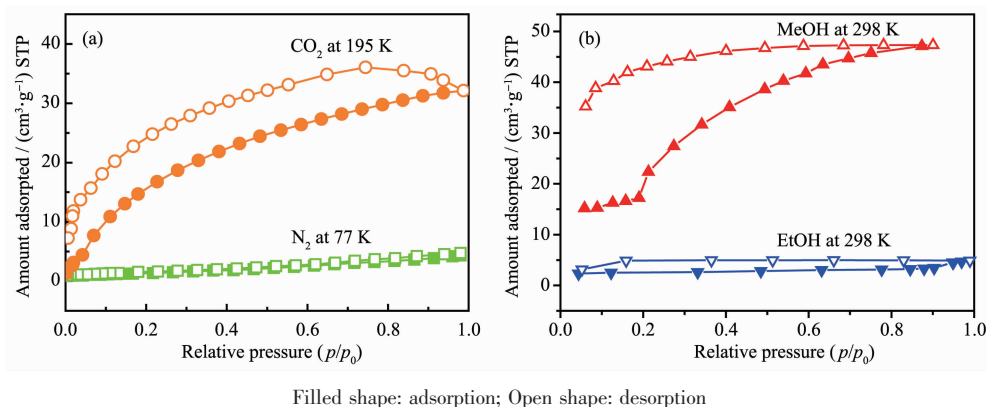Filled shape: adsorption; Open shape: desorption

Fig.4　(a) N_2 at 77 K and CO_2 at 195 K sorption isotherms for **2′**; (b) MeOH and EtOH at 298 K sorption isotherms for **2′**

2.5　Fluorescence sensing properties

MOFs constructed from d^{10}-metal ions and π-conjugated skeleton ligands are usually considered to be potential luminescent materials[30-34]. Accordingly, the luminescence properties of tib, H_3BPT ligands and **1** were studied in the solid state at room temperature.

It was found that **1** displayed apparent fluorescence enhancement and the intense emission bands were observed at λ_{em}=398 nm (λ_{ex}=335 nm) as exhibited in Fig.5, which may be attributed to the tib and H_3BPT ligands emission since the free tib and H_3BPT ligands exhibited emission at 402 and 408 nm (λ_{ex}=295 nm),

respectively[35-36]. It has been reported that the construction of architectures can enhance the rigidity of the aromatic backbone of the ligands and strengthen the intramolecular/intermolecular interactions among the organic ligands, which are beneficial to energy transfer[37]. Compared with the free tib and H3BPT ligands, the observed much stronger emission intensity of **1** implies that the formation of MOFs enhances the fluorescence of the ligand.
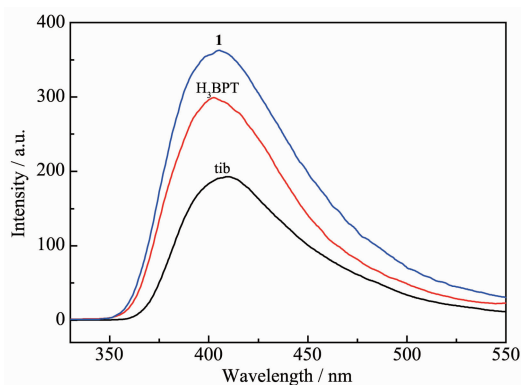

Fig.5　Solid-state photoluminescence spectra of the free tib and H3BPT ligands (λ_{ex}=295 nm) and **1** (λ_{ex}= 335 nm) at room temperature

To examine the potential sensing properties for small organic solvent molecules, the fluorescence experiments of **1** were carried out by dispersing 5 mg well-ground crystalline powder samples in 3 mL different organic solvents including MeOH, EtOH, 2-propanol (2-PA), CH_3CN, DMF, DMA, THF, $CHCl_3$, CH_2Cl_2 and acetone. As illustrated in Fig.6, the intensity of the photoluminescent (PL) of **1** distinctly depended on the identity of the solvent molecule and
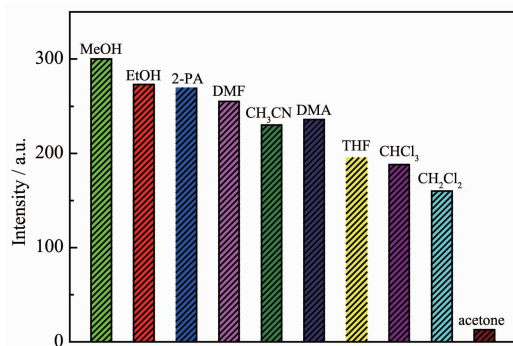

Fig.6　Photoluminescence intensities of **1** introduced into different pure organic solvents when excited at 335 nm

the emission intensity of **1** in MeOH dispersion was stronger than those in other solvent dispersions under the same concentration. Therefore, MeOH was chose as dispersion solvent in the sensing studies. Furthermore, only addition of acetone can quench the fluorescence emissions of **1** efficiently. These experimental phenomena can be mainly attributed to dierent interactions between the framework architecture and distinct organics[38].

To examine the sensing sensitivity of **1** toward acetone in detail, a batch of suspensions of **1** were dispersed in MeOH solution, respectively, with gradually increasing acetone concentration. As exhibited in Fig. 7, with the addition of acetone into the suspensions of **1**, a gradual decrease of the fluorescence intensity was observed. The results of fluorescence titration of **1** show that about 50% decrease of the luminescence intensity was reached with the addition of 5 μL acetone, and the luminescence was almost completely quenched with the addition of 50 μL acetone. Therefore the tib-composed complex **1** may be served as a potential fluorescent sensing material.
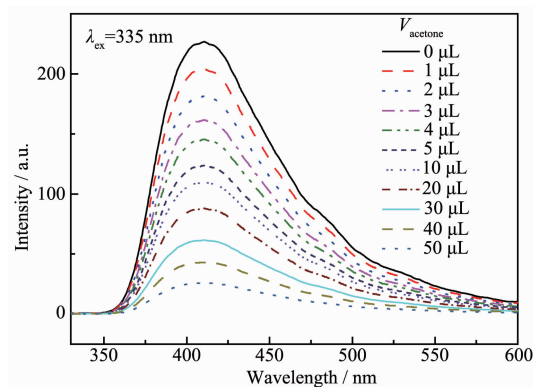

Fig.7　Fluorescence titrations of compound **1** dispersed in 1 mg·mL⁻¹ MeOH with gradual addition of acetone

3　Conclusions

In summary, two new Cd(Ⅱ) and Zn(Ⅱ)-based MOFs with mixed tib and tricarboxylate ligands have been synthesized. Gas/vapor adsorption and luminescence behavior of the complexes were investigated and the results indicate that complexes **1** and **2** both show the ability to selectively adsorb CO_2 over N_2, MeOH over EtOH, suggesting a possible application

in selective gas/vapor adsorption and separation. More importantly, complex **1** shows unique selectivity for detection of acetone through luminescence quenching mechanism. It can be seen that the mixed ligand is an effective strategy for assembling MOF-based functional material.

Supporting information is available at http://www.wjhxxb.cn

References:

[1] Cui X L, Chen K J, Xing H B, et al. *Science*, **2016,353**:141-144

[2] Karim A, Youssef B, Mohamed E. *Chem. Soc. Rev.*, **2017, 46**:3402-3430

[3] Chen S S, Chen M S, Takamizawa S, et al. *Chem. Commun.*, **2011,47**:752-754

[4] Li B Y, Dong X L, Wang H, et al. *Nat. Commun.*, **2017,8**:485-493

[5] Banerjee D, Simonet C M, Thallapally P K, et al. *Nat. Commun.*, **2016,7**:11831-11837

[6] Yin Z, Wan S, Yang J, et al. *Coord. Chem. Rev.*, **2019,378**:500-512

[7] Hughes J T, Sava D F, Nenoff T M, et al. *J. Am. Chem. Soc.*, **2013,135**:16256-16259

[8] Hou C, Liu Q, Fan J, et al. *Inorg. Chem.*, **2012,51**:8402-8408

[9] Li Y L, Zhao Y, Wang P, et al. *Inorg. Chem.*, **2016,55**:11821-11830

[10]Li Y L, Zhao Y, Kang Y S, et al. *Cryst. Growth Des.*, **2016, 16**:7112-7123

[11]Zhang, Z X, Ding N N, Zhang W H, et al. *Angew. Chem. Int. Ed.*, **2014,53**:4628-4632

[12]Ko N, Noh K, Sung S H, et al. *Chem. Commun.*, **2014,50**:6785-6788

[13]Su Z, Fan J, Chen M, et al. *Cryst. Growth Des.*, **2011,11**:1159-1169

[14]Su Z, Fan J, Chen M, et al. *Cryst. Growth Des.*, **2010,10**:3515-3521

[15]Hua J A, Zhao Y, Kang Y S, et al. *Dalton Trans.*, **2015,44**:11524-11532

[16]Fan J, Gan L, Kawaguchi H, et al. *Chem. Eur. J.*, **2003,9**:3965-3973

[17]*SAINT, Program for Data Extraction and Reduction*, Bruker AXS, Inc., Madison, WI, **2001**.

[18]Sheldrick G M. *SADABS*, University of Göttingen, Germany, **1996**.

[19](a)Sheldrick G M. *SHELXT*-2014, *Program for the Crystal Structure Solution*, University of Göttingen, Germany, **2014**.

(b)Sheldrick G M. *SHELXL*-2014, *Program for the Crystal Structure Solution*, University of Göttingen, Germany, **2014**.

[20]Sheldrick G M. *SHELXL*-2018, *Program for the Crystal Structure Solution*, University of Göttingen, Germany, **2018**.

[21]Spek A L. *Acta Crystallogr. Sect. A*, **1990,A46**:194-196

[22]Spek A L. *PLATON, A Multipurpose Crystallographic Tool*, Utrecht University, The Netherlands, **2005**.

[23]Blatov V A. *TOPOS, A Multipurpose Crystallochemical Analysis with the Program Package*, Samara State University, Russia, **2009**.

[24]Blatov V A. *IUCr Comp. Comm. Newslett.*, **2006,7**:4-38

[25]Choi H S, Suh M P. *Angew. Chem. Int. Ed.*, **2009,48**:6865-6869

[26]Hou C, Liu Q, Lu Y, et al. *Microporous Mesoporous Mater.*, **2012,152**:96-103

[27]Chen M S, Chen S S, Takamizawa, et al. *Chem. Commun.*, **2011,47**:3787-3789

[28]Zhong D C, Zhang W X, Cao F L, et al. *Chem. Commun.*, **2011,47**:1204-1206

[29]Higuchi M, Tanaka D, Horike S, et al. *J. Am. Chem. Soc.*, **2009,131**:10336-10337

[30]He K H, Song W C, Li Y W, et al. *Cryst. Growth Des.*, **2012, 12**:1064-1068

[31]Zeng M H, Yin Z, Liu Z H, et al. *Angew. Chem. Int. Ed.*, **2016,55**:11407-11411

[32]Yin Z, Zhou Y L, Zeng M H, et al. *Dalton Trans.*, **2015,44**:5258-5275

[33]Barsukova M, Goncharova T, Samsonenko D, et al. *Crystals*, **2016,6**:132-147

[34]Barsukova M O, Sapchenko S A, Kovalenko K A, et al. *New J. Chem.*, **2018,42**:6408-6415

[35]Wang X L, Bi Y F, Liu G C, et al. *CrystEngComm*, **2008,10**:349-356

[36]Zhang L, Li Z J, Lin Q P, et al. *Inorg. Chem.*, **2009,48**:6517-6525

[37]Zheng X F, Zhou L, Huang Y M, et al. *J. Mater. Chem. A*, **2014,2**:12413-12422

[38]Bauer C A, Timofeeva T V, Settersten T B, et al. *J. Am. Chem. Soc.*, **2007,129**:7136-7144